

An electron–positron beam–plasma instability

S. J. Gilbert, Daniel H. E. Dubin, R. G. Greaves,^{a)} and C. M. Surko

University of California, San Diego, Department of Physics, 9500 Gilman Drive, La Jolla, California 92093-0319

(Received 19 April 2001; accepted 7 August 2001)

Using a new technique to generate cold electron beams, an electron-beam positron-plasma experiment was performed in a previously unexplored range of energies. An electron beam, formed from a thermalized room-temperature electron plasma, is transmitted through a positron plasma stored in a quadrupole Penning trap geometry. The transit-time instability, which is excited by the beam, was previously studied using a hot-cathode electron gun. The large beam energies produced by the cathode did not permit an investigation of the instability in the interesting range of energies near its onset. Using a new 0.1 eV energy width electron beam, we have reinvestigated the system. The experimental data are compared with the results of a theoretical model, also described in this paper. The theory employs a linearized cold fluid and Vlasov approach to model the plasma and beam dynamics, respectively. The data and predictions are in good agreement over the broad range of energies and beam currents studied. © 2001 American Institute of Physics.

[DOI: 10.1063/1.1407284]

I. INTRODUCTION

Electron–positron plasmas are examples of a larger class of equal-mass plasmas (or pair plasmas) that owe their unique properties to the symmetry between the two oppositely charged species. Electron–positron plasmas, in particular, have been extensively studied theoretically because of their relevance in astrophysical contexts such as pulsar magnetospheres.¹ The linear properties of these plasmas are well known.^{2–4} Their nonlinear properties are currently the focus of theoretical and numerical investigations.^{5–15}

Studies of electron–positron plasmas in the laboratory present substantial challenges to the experimentalist. Until recently, insufficient numbers of positrons were available to create even single-component positron plasmas. With the introduction of a modified Penning–Malmberg trap and buffer-gas technique used for accumulating large numbers of positrons,¹⁶ it became possible to conduct the first electron–positron plasma experiments in a beam–plasma system.¹⁷ Unfortunately, the accumulation of large numbers of positrons is possible only because of the outstanding confinement properties of Penning traps,¹⁸ which can confine only one sign of charge. The creation of an electron–positron plasma in the laboratory requires solving the classic plasma physics problem of neutral plasma confinement, and none of the current configurations for confining neutral plasmas has sufficiently good confinement for electron–positron plasmas.

One possible approach to creating equal-mass plasmas is to use positive and negative ions rather than electrons and positrons. Plasmas containing both positive and negative ions are relatively easy to create by the well-known method of producing a hot-cathode discharge in a mixture of electronegative and electropositive gases such as sulfur hexafluoride and argon. Positive ions are created by ionization of the

argon and negative ions are created by electron attachment to the sulfur hexafluoride.¹⁹ Unfortunately, for the experiments conducted to date, there was a rather large mass ratio between the ions (140:40 for SF₆ and Ar), and so these plasmas are not strictly equal-mass plasmas. Even if it were possible to obtain a more nearly equal mass ratio by the judicious choice of gases, a fundamental problem remains: it is currently impossible to entirely eliminate the small residual electron component, which can completely alter the properties of such plasmas, even in concentrations of less than 1%. Plasmas of this type are therefore properly considered to be three-component plasmas.

Using another approach, Schermann and Major created an electron-free plasma consisting of positive and negative ions of (almost) equal mass in a Paul trap by ionizing thallium iodide to create Tl⁺ and I[−] ions.²⁰ The deconfining effects of rf heating were overcome by the cooling effect of a light buffer gas, helium. For electron–positron plasmas, this approach is much less attractive, because the cooling effect of helium for light particles will be minimal. This approach may work, however, by using a molecular species with a high inelastic cross section to provide the required energy loss mechanism. On the basis of current knowledge of positron–molecule collision cross sections, the vibrational excitation of carbon tetrafluoride is the most attractive candidate.²¹ In addition to the Paul trap, other approaches to confine equal-mass plasmas have also been investigated, including the use of combined traps,²² magnetic mirrors,²³ and nested traps.²⁴

Nonetheless, all of these techniques are still relatively complicated, and were not attempted for the experiments described in this paper. Instead, we approached the experimental study of the electron–positron plasmas by investigating the electron–positron beam–plasma system. This approach involves transmitting the abundant species (the electrons) in a single pass through the scarce species (the positrons) con-

^{a)}First Point Scientific, Inc., Agoura Hills, California 91301.

finned in a Penning trap. This permits us to take advantage of the good confinement properties of positron plasmas in Penning traps, while still studying a two-component equal-mass system.

The beam–plasma system is interesting in its own right. The free energy in the relative streaming of the two species can give rise to a variety of instabilities and consequent plasma heating.²⁵ These effects can be important in a variety of laboratory, magnetospheric, and astrophysical plasmas. Beam–plasma effects are currently being investigated theoretically for electron–positron plasmas in the context of wave generation and particle acceleration.^{6–9} The transit-time instability, which is the subject of this paper, was first studied because of its potential as a source of microwave radiation.^{26,27}

The data described in this paper represent a second generation beam–plasma experiment. In our earlier experiments, an electron beam formed from a hot cathode was transmitted through a positron plasma stored in both a cylindrical and quadrupole Penning trap geometry. In the cylindrical case, a two-stream instability was studied, which caused strong heating of the plasma. When the electron beam was passed through a positron plasma stored in a quadrupole Penning trap, the electron beam produced a transit-time instability that excited the center of mass mode in the plasma. Because of the large energy spread generated by the hot-cathode electron gun, both experiments were restricted to studying the instabilities at energies above ~ 1 eV. However, theoretical predictions for both the cylindrical²⁸ and quadrupole (see Sec. II) trap geometries showed that the maximum growth rate and onset of the instability should occur below this energy. It was clear, therefore, that an electron beam with a narrower energy spread would greatly improve our ability to study the instabilities in the energy range near their onset.

Unfortunately, conventional methods used to improve the energy resolution of a hot-cathode beam, such as $E \times B$ filters and spherical deflectors will not work in the strong magnetic field (~ 1200 G) needed for the radial confinement of the positron plasma. In fact, one can show that for the beam currents of the order needed for these experiments ($\sim 0.3 \mu\text{A}$), the lower limit of the energy resolution is 0.1 eV, even for a nonmagnetized beam.²⁹ It is, therefore, nontrivial to produce the required electron currents necessary for the beam–plasma experiment with an energy resolution significantly better than 1 eV. We have been able to overcome these limitations using a novel technique that we developed specifically for producing a high-current cold magnetized electron beam (0.1 eV at 0.1 μA). In this paper we discuss the first application of this beam, using it to further investigate the transit-time instability for a positron plasma stored in a quadrupole well. New results are presented exploring the instability in the previously uninvestigated energy range down to the low-energy onset of the instability. These results are discussed along with a new analytical theory that accurately models the system. The theory describes the plasma dynamics using a cold-fluid approach while the perturbed beam density is modeled using a one-dimensional guiding-center Vlasov equation. Possible future beam–plasma experiments

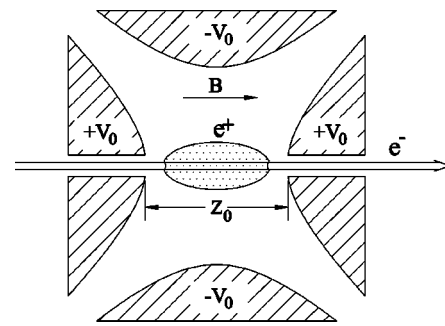


FIG. 1. Schematic diagram of the transit-time instability experiment showing the cross section of an ideal quadrupole Penning trap, truncated for convenience. An electron beam is shown interacting with a positron plasma, located on the trap axis.

in both the cylindrical and quadrupole Penning traps are also discussed.

This paper is structured as follows. In Sec. II, a theoretical model used to describe the transit-time instability will be discussed. The details of the experimental apparatus and techniques used to perform the experiments are presented in Sec. III. In Sec. IV we discuss the experimental results and compare them with the theory. In Sec. V, future research directions are described. Finally, a summary and concluding remarks are presented in Sec. VI.

II. THEORY OF THE TRANSIT-TIME INSTABILITY

The transit-time instability described here is excited when an electron beam interacts with the oscillating field of a plasma center-of-mass mode. For this experiment a non-neutral plasma is stored in a quadrupole well creating a center-of-mass mode, with a high- Q resonance. Figure 1 shows an idealized schematic diagram of the beam–plasma experiment. For certain values of $\omega_z \tau$, where ω_z is the center-of-mass oscillation frequency, and τ is the charged particles transit time through the positron plasma, energy can be extracted from the beam to drive the center-of-mass oscillations. This instability is similar to the transit-time effects that occur in diodes, triodes, and klystrons used to generate microwave radiation.^{26,27} The following is a more detailed description of the analytical theory used to model the system.

A weak, cold electron beam is directed axially through a cold single species non-neutral plasma consisting of N_p particles of charge q and mass M . The beam interacts with the cold fluid normal modes of the plasma, in particular, the axial center-of-mass oscillation. In a quadrupole well the plasma center-of-mass mode has an oscillation frequency corresponding to that of a single positron oscillating in the well. This frequency is given by $\omega_z = \sqrt{8qV_0/MZ_0^2}$, where $2V_0$ is the potential difference applied between the hyperbolic electrodes used to generate the quadrupole potential, and Z_0 is a length parameter that is defined by the electrode geometry (see Fig. 1).³⁰ For the experiments presented here $V_0 \approx 0.025$ statvolts (7.5 V) and $Z_0 \approx 12.6$ cm, corresponding to a frequency of $\omega_z/2\pi \approx 4.1$ MHz.

In this section we determine the shift in the frequency of this oscillation due to the electron beam. We find that the frequency shift is complex, with an imaginary part whose

sign depends on both the shape and size of the plasma as well as the beam current and velocity. For certain combinations of these parameters, the imaginary part of the frequency shift is positive, indicating instability.

We first consider the plasma equilibrium, and then examine the dynamics. In the absence of the electron beam, the plasma is assumed to be in a confined thermal equilibrium state.³¹ This state is described by uniform temperature and rotation frequency ω_r , where ω_r is given by the roots of the equation $\omega_p^2 = 2\omega_r(\Omega_c - \omega_r)$. At low temperatures (such that the plasma Debye length is small compared to the plasma size) the plasma density is also uniform, given by $n_0 = M\omega_r(\Omega_c - \omega_r)/(2\pi q^2)$, where Ω_c is the cyclotron frequency of the plasma charges. In a quadrupole trap, the plasma shape is a spheroid, with diameter $2R_p$ and length $2Z_p$ determined by the external trap fields, the rotation frequency ω_r , and N_p :

$$\frac{4}{3}\pi n_0 R_p^2 Z_p = N_p, \tag{1}$$

$$2 \frac{\omega_z^2}{\omega_{p_0}^2} = A_3(\alpha), \tag{2}$$

where $\omega_{p_0}^2 = 4\pi q^2 n_0 / M$ is the plasma frequency, $\alpha = Z_p / R_p$ is the aspect ratio of the spheroidal plasma, and $A_3(\alpha)$ is the following function:

$$A_3(\alpha) = \frac{2Q_1^0(\alpha/\sqrt{\alpha^2-1})}{(\alpha^2-1)}, \tag{3}$$

where $Q_n^0(x)$, a Legendre function of the second kind, with the branch cuts chosen so that $Q_n^0(x)$ vanishes for $x \rightarrow \infty$. Equation (1) is merely a statement of the relation between the volume and the major and minor radii of a spheroid, and Eq. (2) arises from the equilibrium condition that the electrostatic potential be z independent within the plasma:

$$\frac{\partial}{\partial z} [\phi_{p_0}^{\text{in}}(r,z) + \phi_{\text{ext}}(r,z)] = 0, \tag{4}$$

where $\phi_{\text{ext}}(r,z)$ is the quadrupole trap field:

$$\phi_{\text{ext}}(r,z) = \frac{1}{2} \frac{M\omega_z^2}{q} \left(z^2 - \frac{1}{2} r^2 \right), \tag{5}$$

and $\phi_{p_0}^{\text{in}}(r,z)$ is the equilibrium electrostatic potential due to the plasma alone, evaluated inside the plasma:³¹

$$\phi_{p_0}^{\text{in}}(r,z) = - \frac{M\omega_{p_0}^2}{4q} (A_1 r^2 + A_3 z^2 - 2A_1 R_p^2 - A_3 Z_p^2), \tag{6}$$

and $A_1(\alpha) = 1 - A_3(\alpha)/2$.

We will also have need of the equilibrium plasma potential outside the spheroid:

$$\phi_{p_0}^{\text{out}}(r,z) = a_0 Q_0^0(\xi_1/d) + a_2 P_2(\xi_2) Q_2^0(\xi_1/d), \tag{7}$$

where $P_2(x)$ is a Legendre polynomial, (ξ_1, ξ_2) are spheroidal coordinates given in terms of cylindrical coordinates by the transformation

$$z = \xi_1 \xi_2, \tag{8a}$$

$$r = \sqrt{(1 - \xi_2^2)(\xi_1^2 - d^2)}, \tag{8b}$$

$d = \sqrt{Z_p^2 - R_p^2}$, and a_0 and a_2 are constants obtained by matching the interior and exterior solutions for ϕ_{p_0} :

$$a_0 Q_0^0 \left(\frac{\alpha}{\sqrt{\alpha^2-1}} \right) = \frac{M\omega_z^2 Z_p^2}{3q} \left(\frac{2A_1}{\alpha^2 A_3} + 1 \right), \tag{9a}$$

$$a_2 Q_2^0 \left(\frac{\alpha}{\sqrt{\alpha^2-1}} \right) = \frac{M\omega_z^2 Z_p^2}{3q} \left(\frac{A_1}{\alpha^2 A_3} - 1 \right). \tag{9b}$$

The spheroidal plasma equilibrium described above has a large number of stable normal modes of oscillation. These modes can be described analytically. The simplest mode, and the one of interest here, is the axial center-of-mass oscillation. This mode consists of an axial harmonic oscillation of the plasma center of mass without any change in plasma shape. The resulting plasma potential $\phi_p(r,z,t)$ is described by a shifted equilibrium potential:

$$\begin{aligned} \phi_p(r,z,t) &= \phi_{p_0}[r,z - Z_c(t)] \\ &\approx \phi_{p_0}(r,z) - Z_c(t) \frac{\partial \phi_{p_0}(r,z)}{\partial z}, \end{aligned} \tag{10}$$

where $Z_c(t) = |Z_0| \cos(\omega_z t + \theta)$ is the center-of-mass position, $\phi_{p_0}(r,z)$ is given by Eqs. (6) and (7), and the Taylor expansion is warranted for small (linear) oscillations, providing a perturbed mode potential $\delta\phi(\mathbf{r},t) = \phi_p(r,z,t) - \phi_{p_0}(r,z)$:

$$\delta\phi^{\text{in}}(\mathbf{r},t) = \frac{M\omega_z^2}{q} Z_c(t) z, \tag{11}$$

inside the plasma and

$$\delta\phi^{\text{out}}(\mathbf{r},t) = \frac{M\omega_z^2}{q} Z_c(t) Z_p \xi_2 \frac{Q_1^0(\xi_1/d)}{Q_1^0(\alpha/\sqrt{\alpha^2-1})}, \tag{12}$$

outside the plasma.

We now consider the effect of the electron beam on the plasma equilibrium and dynamics. The spheroidal equilibrium plasma described above is perturbed to a new equilibrium when the electron beam is turned on. We are concerned here with the stability of this new equilibrium. The form of the new equilibrium is somewhat complex but fortunately, for a weak beam, we do not require it in order to determine stability. Nevertheless, a brief qualitative description of the new equilibrium may be of interest.

The electron beam has higher density inside the plasma than outside, because the electron velocity falls off as electrons approach the plasma (the external trap field is confining for positrons, repulsive for electrons). The density variation of the beam acts to attract plasma positrons toward the trap center along the magnetic field, with the result that plasma density is enhanced in the region of the beam. The density enhancement is accomplished by a decrease in plasma length, creating ‘‘dimples’’ at the plasma ends (see Fig. 1). However, when the beam current I_b is sufficiently small so that $I_b/(qN_p\omega_z) \ll 1$, we will see that these effects on the plasma equilibrium can be neglected when examining questions of stability. Nevertheless, the increased axial confine-

ment provided by the beam produces an enhancement to the real frequency of the center of mass oscillation, which we will determine.

In order to evaluate the effect of the electron beam on the frequency of the center-of-mass mode, we first consider the equation of motion for the plasma center of mass, $Z_c(t)$:

$$MN_p \frac{d^2 Z_c}{dt^2} = F_{z_{\text{ext}}} + F_{z_{\text{beam}}}, \tag{13}$$

where $F_{z_{\text{ext}}}$ is the total force on the plasma in the z direction due to the external trap potential, and $F_{z_{\text{beam}}}$ is the force due to the electron beam. Note that the plasma cannot exert a total force on itself, and that we neglect the effect of image charges. The external trap force $F_{z_{\text{ext}}}$ can be easily evaluated because of the quadratic form of the trap potential. This force is an integral over the plasma density:

$$F_{z_{\text{ext}}} = - \int d^3 r q n_p(\mathbf{r}, t) \left(\frac{M \omega_z^2}{q} z \right) = - N_p M \omega_z^2 Z_c(t), \tag{14}$$

where the second equality follows from the definition of center of mass.

Similarly, the force from the electron beam is

$$F_{z_{\text{beam}}} = - \int d^3 r q n_p(\mathbf{r}, t) \frac{\partial \phi_b}{\partial z}(\mathbf{r}, t), \tag{15}$$

when $\phi_b(\mathbf{r}, t)$ is the potential due to the beam. This force is, in general, out of phase with $Z_c(t)$, causing growth in the center-of-mass oscillations. In order to investigate this, we treat $Z_c(t)$ as a complex variable:

$$Z_c(t) = Z_0 e^{i\omega t},$$

where ω is the complex frequency of the mode, and $Z_0 = |Z_0| e^{i\theta}$ is the complex amplitude. Substituting Eqs. (14) and (15) into Eq. (13), we arrive at an exact expression for ω :

$$\omega^2 = \omega_z^2 + \frac{q}{MN_p Z_c(t)} \int d^3 r n_p(\mathbf{r}, t) \frac{\partial \phi_b}{\partial z}. \tag{16}$$

This expression can be put in a more useful form by applying Poisson's equation for the electron beam and the plasma,

$$\nabla^2 \phi_p = -4\pi q n_p(\mathbf{r}, t), \tag{17a}$$

$$\nabla^2 \phi_b = 4\pi e n_b(\mathbf{r}, t), \tag{17b}$$

and integrating by parts several times:

$$\omega^2 = \omega_z^2 + \frac{e}{MN_p Z_c(t)} \int d^3 r n_b(\mathbf{r}, t) \frac{\partial \phi_p(\mathbf{r}, t)}{\partial z}. \tag{18}$$

In the limit of a weak beam, the integral provides a small correction to the mode frequency. Since this term is already small, we need not keep corrections to $\phi_p(\mathbf{r}, t)$ from the presence of the beam, and can therefore employ the analytic expressions Eqs. (10), (11), and (12). Furthermore, assuming the beam is narrow compared to R_p allows us to replace the three-dimensional integral in Eq. (18) by a single integral in z :

$$\omega^2 = \omega_z^2 + \frac{e A_b}{MN_p Z_c(t)} \int dz \hat{n}_b(z, t) \frac{\partial \hat{\phi}_p}{\partial z}(z, t), \tag{19}$$

where A_b is the cross-sectional area of the beam, $\hat{\phi}_p(z, t) = \phi_p(r=0, z, t)$, and $\hat{n}_b(z, t)$ is a radial average of the beam density. Substituting Eq. (10) into Eq. (19), we obtain

$$\omega^2 = \omega_z^2 - \frac{e A_b}{MN_p} \int_{-\infty}^{\infty} dz \frac{\partial^2 \hat{\phi}_{p_0}(z)}{\partial z^2} (z) \hat{n}_b(z, t) + \frac{e A_b}{MN_p Z_c(t)} \int_{-\infty}^{\infty} dz \frac{\partial \hat{\phi}_{p_0}(z)}{\partial z} \hat{n}_b(z, t), \tag{20}$$

where $\hat{\phi}_{p_0}(z) = \phi_{p_0}(r=0, z)$. In the first integral, the perturbation to the beam density can be neglected in linear theory, and we can take $\hat{n}_b(z, t) \approx \hat{n}_{b_0}(z)$, the equilibrium (radially averaged) beam density. In the second integral, we recognize that $\hat{n}_{b_0}(z)$ is an even function of z , while $\partial \hat{\phi}_{p_0} / \partial z$ is an odd function of z . Taking $\omega = \omega_z + \Delta \omega$, we can therefore write the frequency shift as a sum of two terms:

$$\Delta \omega = \Delta \omega_1 + \Delta \omega_2,$$

where

$$\Delta \omega_1 = - \frac{e A_b}{2MN_p \omega_z} \int_{-\infty}^{\infty} dz \frac{\partial^2 \hat{\phi}_{p_0}(z)}{\partial z^2} \hat{n}_{b_0}(z) \tag{21}$$

and

$$\Delta \omega_2 = \frac{e A_b}{2MN_p \omega_z} \int_{-\infty}^{\infty} dz \frac{\partial \hat{\phi}_{p_0}(z)}{\partial z} \frac{\delta \hat{n}_b(z, t)}{Z_c(t)}, \tag{22}$$

where $\delta \hat{n}_b(z, t) = \hat{n}_b(z, t) - \hat{n}_{b_0}(z)$ is the perturbed beam density due to the mode. The physical significance of $\Delta \omega_1$ and $\Delta \omega_2$ is clear: $\Delta \omega_1$ is the real frequency shift caused by inhomogeneity of the equilibrium beam density. For uniform beam density, this term vanishes (since $\partial \hat{\phi}_{p_0} / \partial z \rightarrow 0$ at $\pm \infty$). On the other hand, $\Delta \omega_2$ is a frequency shift caused by beam dynamics in the presence of the mode. This frequency shift is complex in general [recall that $Z_c(t)$ is a complex quantity; we will soon see that $\delta \hat{n}_b(z, t)$ is also complex]. Note that $\delta \hat{n}_b(z, t) / Z_c(t)$ is a finite quantity, independent of Z_c , in the limit of an infinitesimal linear mode.

In order to evaluate the frequency shift, we require expressions for the equilibrium beam density $\hat{n}_b(z)$ and the perturbed beam density $\delta \hat{n}_b(z, t)$. If one assumes that the beam is monoenergetic, with energy E_0 , these expressions are easily obtained. The equilibrium beam density can be written in terms of the beam velocity using continuity, assuming that the beam is not reflected at any point:

$$\hat{n}_b(z) = \frac{\Gamma}{v_b(z)}, \tag{23}$$

where Γ is the (constant) equilibrium beam particle flux. The beam velocity $v_b(z)$ is determined by energy conservation:

$$E_0 = \frac{1}{2} m v^2 - e \phi_0(z), \tag{24}$$

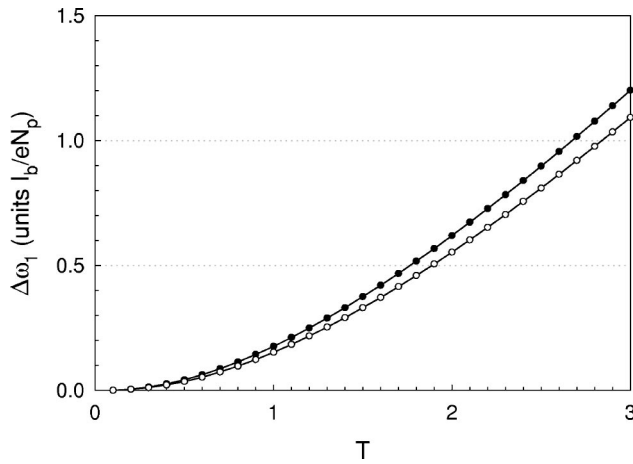


FIG. 2. Real frequency shift, $\Delta\omega_1$, of the center-of-mass oscillation caused by the inhomogeneity of the equilibrium beam density, for a plasma aspect ratio of (●) $\alpha=1.1$ and (○) $\alpha=1.4$. The frequency shift is scaled by I_b/eN_p , where I_b is the beam current and N_p is the number of plasma charges, and is plotted versus the scaled transit time $T = \omega_z Z_p/v_{in}$.

where $\phi_0(z) = \phi_{ext}(r=0,z) + \hat{\phi}_{p_0}(z)$ is the equilibrium electrostatic potential along the trap axis, given by Eqs. (5)–(7). Solving for v , assuming no turning points, yields

$$v_b(z) = \sqrt{\frac{2E_0}{m} + \frac{2e}{m}\phi_0(z)} = \sqrt{v_{in}^2 + \frac{2e}{m}\Delta\phi_0(z)}, \quad (25)$$

where $v_{in} = \sqrt{[2E_0 + e\phi_0(0)]/m}$ is the (constant) beam velocity inside the plasma, and $\Delta\phi_0(z) = \phi_0(z) - \phi_0(0)$. Using Eqs. (2) and (5)–(7) for ϕ_{ext} and ϕ_{p_0} , the frequency shift $\Delta\omega_1$ can be expressed as

$$\Delta\omega_1 = \frac{I_b}{qN_p} TW_1\left(\alpha, \frac{eM}{qm} T^2\right), \quad (26)$$

where $I_b = e\Gamma A_b$ is the beam current, α is plasma aspect ratio, the dimensionless function $W_1(\alpha, y)$ is given by

$$W_1(\alpha, y) \equiv 1 - \int_1^\infty \frac{d\bar{z}}{\bar{v}_b(\bar{z}, \alpha, y)} F(\bar{z}, \alpha), \quad (27)$$

$\bar{v}_b \equiv v_b/v_{in}$, $F \equiv q/(M\omega_z^2)\partial^2\hat{\phi}_{p_0}/\partial z^2$, $\bar{z} \equiv Z/Z_p$, and

$$T \equiv \frac{Z_p}{v_{in}} \omega_z \quad (28)$$

is half the transit time of the beam through the plasma, normalized by ω_z . For the case of interest here, $eM/qm = 1$ (positron plasma and electron beam), $\Delta\omega_1$ is plotted versus the transit time for two different aspect ratios in Fig. 2. As expected from our previous qualitative argument, $\Delta\omega_1$ is positive as the beam inhomogeneity creates an extra potential well for the plasma. Also, $\Delta\omega_1$ approaches zero in the limit of a stiff beam, $T \rightarrow 0$, where the beam density becomes z independent.

In order to determine the frequency shift $\Delta\omega_2$ due to beam dynamics, an expression is needed for the perturbed beam density due to the plasma oscillation. This is most

easily accomplished using the Vlasov equation for the beam distribution, $f_b(z, v, t)$. As usual, the density $\hat{n}_b(z, t)$ is obtained from f via velocity integration:

$$\hat{n}_b(z, t) = \int dv f_b(z, v, t). \quad (29)$$

Breaking f_b into an equilibrium and a perturbation, $f_b = f_{b_0}(z, v) + \delta f(z, v, t)$, the linearized Vlasov equation reads as

$$\frac{\partial \delta f_b}{\partial t} + v \frac{\partial}{\partial z} \delta f_b + \frac{e}{m} \frac{\partial \phi_0}{\partial z} \frac{\partial \delta f_b}{\partial v} + \frac{e}{m} \frac{\partial \delta \phi}{\partial z} \frac{\partial f_{b_0}}{\partial z} = 0, \quad (30)$$

where $\delta\phi$ is the perturbed potential due to the mode.

This equation can be solved for δf_b using the method of characteristics. The characteristics $z'(t')$, $v'(t')$ are defined by

$$\frac{dz'}{dt'} = v', \quad (31)$$

$$\frac{dv'}{dt'} = \frac{e}{m} \frac{\partial \phi_0(z')}{\partial z'}, \quad (32)$$

with “initial” conditions $z'(t) = z$, $v'(t) = v$. In terms of these characteristics the solution for δf_b reads as

$$\delta f_b(z, v, t) = -\frac{e}{m} \int_{-\infty}^t dt' \frac{\partial}{\partial z'} \delta \phi(z', t') \frac{\partial f_{b_0}}{\partial v'}(z', v') \Big|_{z'}. \quad (33)$$

Recall that in the expression for the frequency shift, Eq. (16), we require $\delta n_b = \int dv \delta f_b$ in the presence of a normal mode. Since δf_b is already a small quantity of order $\delta\phi$, the frequency shift can be obtained to lowest order in $\delta\phi$ by neglecting the effect of δf_b on $\delta\phi$ in Eq. (33) and substituting the unperturbed normal mode potential, $\delta\phi(z, t) = -Z_0 e^{i\omega t} \partial \hat{\phi}_{p_0} / \partial z$. We then make a change of variables from t' to z' , writing

$$t' = t + t_0(z, z', E_0), \quad (34)$$

where $t_0(z, z', E_0)$ is the time required to move from z to z' for an electron of energy E_0 :

$$t_0(z, z', E_0) = \int_z^{z'} \frac{dz''}{v_b(z'')}, \quad (35)$$

and v_b is implicitly a function of E_0 through Eq. (25).

Equations (34) and (35) imply that $dt' = dz'/v_b(z', E_0)$. This result, together with Eq. (31), implies $v' = v_b(z', E_0)$, which, in turn, allows us to write

$$\frac{\partial}{\partial v'} \Big|_{z', z} = \frac{\partial v}{\partial v'} \Big|_{z', z} \frac{\partial}{\partial v} \Big|_{z', z} = \frac{v_b(z')}{v} \frac{\partial}{\partial v} \Big|_{z', z}, \quad (36)$$

where we have used Eqs. (24) and (25). The perturbed beam density may then be written as

$$\begin{aligned} \delta \hat{n}_b(z, t) &= \int_{-\infty}^{\infty} dv \delta f_b(z, v, t) \\ &= \frac{e}{m} \int_{-\infty}^z dz' \frac{\partial^2 \hat{\phi}_{p_0}(z')}{\partial z'^2} \int_{-\infty}^{\infty} \frac{dv}{v} Z_0 \\ &\quad \times e^{-i\omega[t+t_0(z, z', E_0)]} \\ &\quad \times \left. \frac{\partial}{\partial v} f_{b_0}[z', v'(v, z', z)] \right|_{z', z}. \end{aligned} \quad (37)$$

We now integrate by parts in v and use the fact that phase space area is conserved in the evolution of f_{b_0} , so that $f_{b_0}(z', v') = f_{b_0}(z, v)$. This yields

$$\begin{aligned} \delta \hat{n}_b(z, t) &= -\frac{e}{m} Z_c(t) \int_{-\infty}^z dz' \frac{\partial^2 \hat{\phi}_{p_0}(z')}{\partial z'^2} \\ &\quad \times \int_{-\infty}^{\infty} dv f_{b_0}(z, v) e^{-i\omega t_0(z, z', E_0)} \\ &\quad \times \left(-\frac{1}{v^2} - \frac{i\omega}{v} \frac{\partial}{\partial v} t_0(z, z', E_0) \right) \Big|_{z', z}, \end{aligned} \quad (38)$$

where $E_0 = E_0(z, v)$ through Eq. (24). The derivative of t_0 appearing in Eq. (38) can be written as

$$\left. \frac{\partial t_0}{\partial v}(z, z', E_0) \right|_{z', z} = -v \int_z^{z'} \frac{dz''}{v_b(z'', E_0)^3} \equiv -v t_1(z, z', E_0), \quad (39)$$

where we have used Eqs. (35) and (25) together with the expression $\partial E_0 / \partial v|_z = mv$, which follows from Eq. (24).

Equation (38) is a general expression for the perturbed beam density caused by an oscillating potential, good for any equilibrium beam distribution $f_{b_0}(z, v)$ (provided that no reflections of beam particles occur). The equation simplifies further when a monoenergetic distribution is used, $f_{b_0}(z, v) = \hat{n}_b(z) \delta[v - v_b(z)]$. An evaluation of the velocity integral then yields.

$$\begin{aligned} \delta \hat{n}_b(z, t) &= \frac{e\Gamma}{mv_b(z)} Z_c(t) \\ &\quad \times \int_{-\infty}^z dz' \frac{\partial^2 \hat{\phi}_{p_0}(z')}{\partial z'^2} e^{-i\omega t_0(z, z', E_0)} \\ &\quad \times \left(\frac{1}{v_b^2(z)} - i\omega t_1(z, z', E_0) \right), \end{aligned} \quad (40)$$

where we have used Eq. (23).

When Eq. (40) is substituted in our expression for the frequency shift $\Delta\omega_2$, Eq. (22), we obtain

$$\Delta\omega_2 = \frac{I_b}{qN_p} W_2 \left(\alpha, T, \frac{eM}{qm} \right), \quad (41)$$

where the dimensionless function W_2 is given by

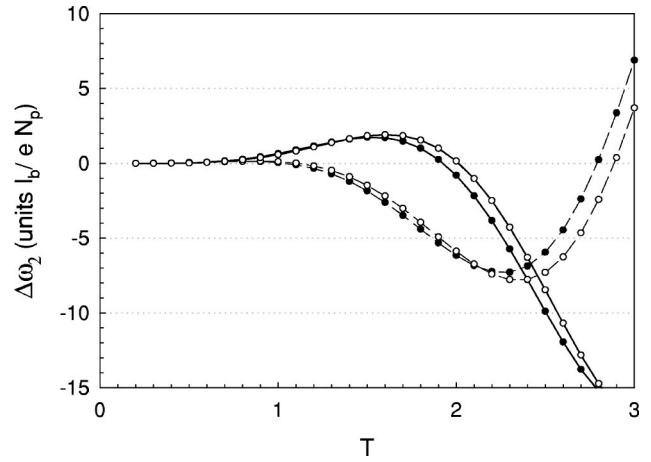


FIG. 3. Real (dashed lines) and imaginary (solid lines) parts to the frequency shift $\Delta\omega_2$ of the center-of-mass oscillation in the presence of an electron beam, for a plasma aspect ratio of (●) $\alpha=1.1$ and (○) $\alpha=1.4$ [see Eq. (41)]. The frequency shift is plotted versus the scaled transit time $T = \omega_z Z_p / v_{in}$.

$$\begin{aligned} W_2(\alpha, T, x) &= \frac{T^3 x}{2} \int_{-\infty}^{\infty} \frac{d\bar{z}}{\bar{v}_b(\bar{z}, \alpha, x T^2)} G(\bar{z}, \alpha) \\ &\quad \times \int_{-\infty}^{\bar{z}} d\bar{z}' e^{-iT\bar{t}_0(\bar{z}, \bar{z}', \alpha, x T^2)} F(\bar{z}', \alpha) \\ &\quad \times \left(-iT\bar{t}_1(\bar{z}, \bar{z}', \alpha, x T^2) + \frac{1}{\bar{v}_b^2(\bar{z}, \alpha, x T^2)} \right), \end{aligned} \quad (42)$$

and where, as before, $\bar{z} = z/Z_p$, $\bar{v}_b = v_b/v_{in}$, $F = q/(M\omega_z^2) \partial^2 \hat{\phi}_{p_0} / \partial z^2$, and $T = Z_p \omega_z / v_{in}$. Also, $G = q/(M\omega_z^2 Z_p) \partial \hat{\phi}_{p_0} / \partial z$, $\bar{t}_0 = t_0 Z_p / v_{in}$, and $\bar{t}_1 = t_1 Z_p / v_{in}^3$, where t_0 and t_1 are given by Eqs. (35) and (39). The dependence of the scaled variables \bar{t}_0 , \bar{t}_1 and \bar{v}_b on aspect ratio α and the combination $eMT^2/(qm)$ follows from the definition of $v_b(z)$, Eq. (25), and the form of the equilibrium trap potential, Eqs. (2), (5)–(7).

The frequency shift is plotted in Fig. 3 as a function of the scaled transit time T for two values of the plasma aspect ratio, $\alpha=1.1$ and $\alpha=1.4$, and for $eM/qm=1$, the case of interest for an electron–positron system. The real part of $\Delta\omega_2$, together with ΔW_1 , determines a shift in the real frequency of the center-of-mass mode, while the imaginary part of $\Delta\omega_2$ determines the growth (for the positive imaginary part) or damping (for the negative imaginary part) caused by the beam. For short transit times (high beam velocity) the mode is unstable, with growth rate scaling as T^5 . This follows from Eq. (42), taking $e^{iT\bar{t}_0} \approx 1$, $\bar{t}_1 \approx \bar{z}' - \bar{z}$, and $\bar{v}_b \approx 1$. For longer transit times, the growth rate and frequency shift display growing oscillations, reflecting the role of phase interference between perturbations in the beam and the normal mode oscillation.

III. DESCRIPTION OF THE EXPERIMENT

Figure 4(a) shows a schematic drawing of the beam–plasma experiment. The apparatus consists of a cylindrical

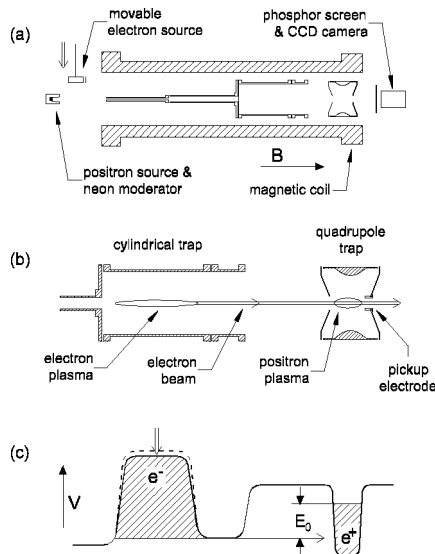


FIG. 4. (a) Schematic diagram of the beam–plasma experiment showing the ^{22}Na positron source and moderator, movable hot-cathode electron source, magnetic field coil, imaging system, and trap electrode structures. (b) Expanded diagram of the cylindrical and quadrupole Penning traps. Each trap consists of three electrodes from left to right, referred to as the entrance-gate, dump, and exit-gate electrodes. The quadrupole trap also has a small pickup electrode located near the positron plasma. (c) Schematic diagram of the potential profile $V(z)$ used to contain the electrons and positrons in their respective potential wells.

Penning–Malmberg trap coaxial with a quadrupole Penning trap. Both traps are enclosed in the same vacuum vessel and in the same confining magnetic field ($B=1200\text{ G}$). As shown in Figs. 4(a) and 4(b), the cylindrical trap is the third stage of a three-stage trap designed to capture positrons from a radioactivity source. The details of the first two stages are described in Ref. 32 but are not relevant to the present paper.

The procedure for conducting the experiment can be split into three phases: (1) the accumulation of a cold positron plasma, which is stored in the quadrupole trap; (2) the accumulation of a reservoir of thermalized electrons stored in the cylindrical trap, and the extraction of an electron beam from this reservoir; and (3) the measurement of the excitation of the transit-time instability in the positron plasma by the electron beam. A more detailed explanation of these three phases is presented below.

A. Positron plasma formation

A high-energy positron from a $90\text{ mCi }^{22}\text{Na}$ source are moderated to about 1.5 eV using a solid neon moderator [see Fig. 4(a)].³³ The moderated positrons are then trapped in the three stage cylindrical penning trap at a rate of 6×10^5 positrons per second by a series of inelastic collisions with a nitrogen buffer gas.^{16,32,34} A plasma containing 1.6×10^7 positrons is accumulated and then shuttled into the quadrupole trap at an efficiency of 80%. The plasma in the quadrupole trap cools to room temperature (0.025 eV) in approximately 1 s by further collisions with the nitrogen buffer gas.³⁴ The buffer gas is then pumped out to a base pressure of $5 \times 10^{-9}\text{ Torr}$ in 10 s .

In order to confirm that the accumulated positrons are in the plasma state, it is necessary to obtain plasma parameters

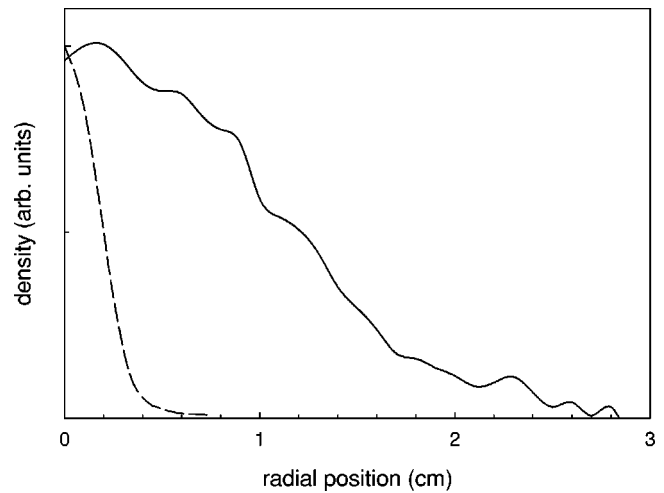


FIG. 5. Axially integrated radial density profile of a plasma containing 1.3×10^7 positrons (solid line). Also shown is the radial profile of the electron beam (dashed line), which is formed from a cold plasma containing 1×10^9 electrons. As discussed in the text these profiles indicate a positron plasma diameter of $D_p \approx 2.4\text{ cm}$ and an electron beam diameter of $D_b \approx 0.4\text{ cm}$.

such as the Debye length and the dimensions of the charge cloud. These parameters were not measured directly, but inferred from measurements of the axial-integrated plasma density profile. This is accomplished by dumping the plasma onto a phosphor screen biased to -10 kV , which is then imaged using a charge-coupled device (CCD) camera [see Fig. 4(a)]. The solid line in Fig. 5 shows a typical axial-integrated radial density profile of a plasma containing 1.3×10^7 positrons. The dashed line represents the narrower density profile of the electron beam, which will be described in Sec. III B. The radial density profile of the plasma is used as input to a Poisson–Boltzmann equilibrium code to calculate the spatial distribution of the positrons in the trap.

The results of this calculation are displayed in Fig. 6(a), which shows the positron number density as a function of position in the plasma. This analysis yields a plasma length of $L_p \approx 3.4\text{ cm}$ full width half-maximum (FWHM) and a diameter of $D_p \approx 3.2\text{ cm}$ FWHM. These dimensions corresponds to a plasma aspect ratio of $\alpha = L_p/D_p \approx 1.1$. We note that the plasma diameter calculated in this way is slightly larger than the plasma diameter obtained from the data shown in Fig. 5. This is due to the line-integrated nature of the CCD camera image, versus the three-dimensional positron density profile shown in Fig. 6(a).

Figure 6(b) compares the positron number density as a function of position along the trap axis of symmetry for the results of the Poisson–Boltzmann simulation (solid line) and the profile used in the theoretical calculation (dotted line). In this case the length of the flat-top profile used in the theory was determined by the FWHM of the Poisson–Boltzmann profile. For more details see Sec. IV. The figure indicates a central plasma density of $n_p \approx 6 \times 10^5\text{ cm}^{-3}$, yielding a Debye length of $\lambda_D \approx 1.5\text{ mm}$. Comparing the Debye length with the plasma dimensions, we see that $\lambda_D \ll L_p$, $\lambda_D \ll D_p$, and $N_D \sim 10^4 \gg 1$, where N_D is the number of positrons in a

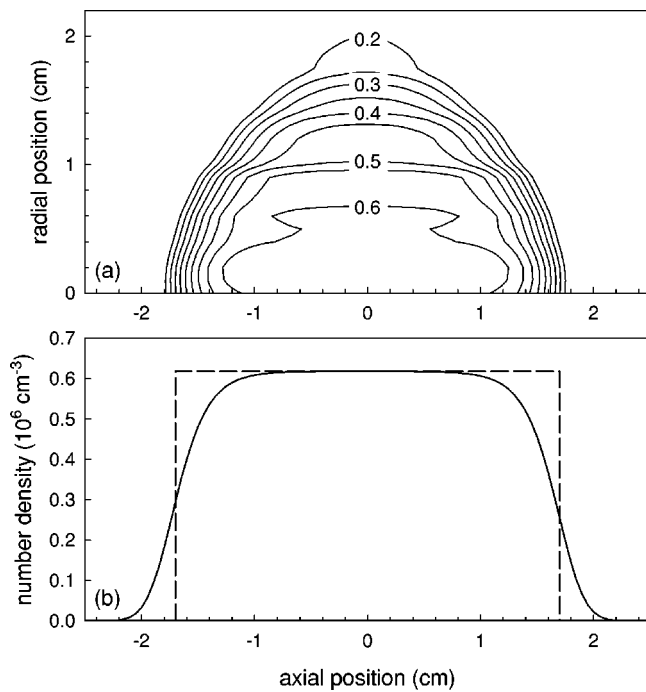


FIG. 6. (a) Contour plot of the density of a 1.3×10^7 positron plasma (in units of $1 \times 10^6 \text{ cm}^{-3}$) stored in the quadrupole well. (b) A comparison of the positron number density along the trap axis (solid line) obtained by the Poisson–Boltzmann calculation and (dashed line) the distribution assumed in the theoretical calculation.

Debye sphere. Thus, the charge cloud satisfies all of the conditions to be a single-component plasma. As discussed in Sec. II, some of the aforementioned plasma parameters can be obtained by the magnetic field strength, total number of trapped positrons, and quadrupole trap parameters Z_0 and V_0 . A comparison between these derived parameters and the measured parameters is shown in Table I, and good agreement is observed.

The last parameter needed for the analysis of the experiment is the space charge potential of the plasma. It is important to determine this parameter because it affects the energy of the electron beam as it passes through the plasma (see Sec. III C). The space charge potential is determined by dumping the plasma and measuring the potential difference on the dump electrode at the start and stop of the dump, as defined by the potential when the positrons start exiting the trap and

TABLE I. Summary of the positron plasma parameters.

Parameter	Derived	Measured
D_p (cm)	3.48	3.2
L_p (cm)	3.37	3.4
$\alpha = L_p / D_p$	0.97	1.1
N	...	1.3×10^7
n_p (cm^{-3})	6.1×10^5	6×10^5
λ_D (mm)	1.5	...
B (G)	...	1200
$\Omega_e / 2\pi$ (GHz)	2.8	...
$\omega_p / 2\pi$ (MHz)	7.0	...
$\omega_z / 2\pi$ (MHz)	4.1	4.2
$\omega_r / 2\pi$ (KHz)	8.8	...

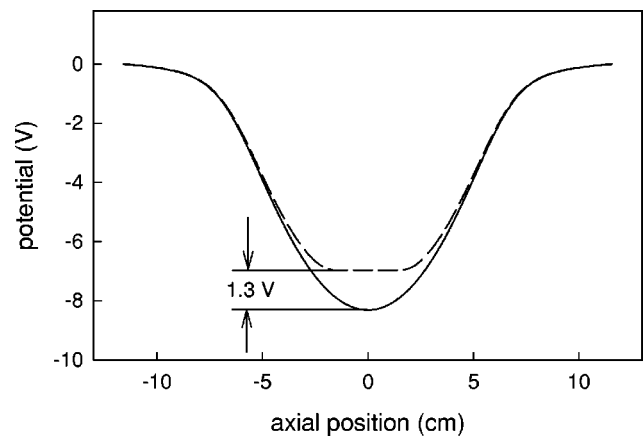


FIG. 7. The potential profile along the axis of symmetry of the trap without any charge present (solid line), and with 1.3×10^7 positrons (dashed line). The difference in potential between the two plots at the center is due to the plasma space charge potential of 1.3 V.

the potential when all the positrons have been expelled, respectively. For the plasmas used in this experiment, a space charge of 1.6 V is typically measured. In order to verify this direct measurement of the space charge, the Poisson–Boltzmann code was used to calculate it. Figure 7 shows the potential profile of the quadrupole trap along its axis of symmetry with and without a positron plasma present. The difference between the two curves represents the positron plasma space charge of ~ 1.3 V for a plasma containing 1.3×10^7 positrons. The discrepancy between the space charge measurement and calculation may be caused by uncertainties in the measured total number of positrons, which is needed in the Poisson–Boltzmann code. Another possible source of error is the measurement of the start and stop of the dump, due to the sensitivity of these measurements in determining the space charge potential.

B. Cold electron beam formation

Following the accumulation of a positron plasma in the quadrupole trap, a cold electron beam is generated. This requires two steps. First electrons are accumulated in the cylindrical Penning trap, shown in Fig. 4(b), and then this reservoir of electrons is used to form an intense cold beam. A hot-cathode electron gun is used as a source of electrons. The extraction voltage on the electron gun is set so that the emission current is $\sim 2 \mu\text{A}$. The electrons are injected along the magnetic field into the cylindrical trap, where they are trapped without the use of a buffer gas via electron–electron collisions. Using a nitrogen buffer gas while accumulating the electrons does increase the trapping efficiency. Unfortunately, this also greatly accelerates the radial transport, resulting in an increased electron beam diameter, which should be small compared to the positron plasma size. In order to maximize the trapping efficiency without a buffer gas, the depth of the confining well is gradually increased as the plasma space charge builds up, so that an approximately constant trapping potential is maintained. While the electrons are being trapped, the potential on the exit-gate electrode of the cylindrical trap is set sufficiently low so that the hot-cathode

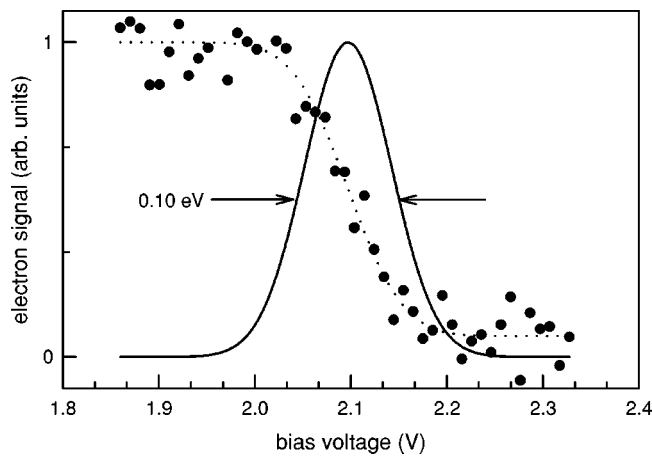


FIG. 8. Energy distribution of a $0.1 \mu\text{A}$ quasi-steady-state electron beam extracted from the Penning trap. Filled circles are the data measured using a cylindrical RPA, and the dotted line is an error-function fit to the data. The solid line, which represents the energy distribution, is the derivative of this fit.

electron beam is separated from the positron plasma stored in the adjacent quadrupole trap. A final well depth of 90 V is reached in ~ 1 s, confining an electron plasma of 3×10^9 electrons with a space charge of 90 V. The trapped electrons then cool to room temperature by collisions with the surrounding neutral background gas.

After an electron plasma has been accumulated in the trap, a cold beam is generated by continuously reducing the depth of the potential well confining the electrons. As the magnitude of the potential well decreases, the electrons are forced over the exit-gate electrode, which sets the electron beam energy [see Fig. 4(c)]. The entrance-gate electrode is set 1 V below the exit-gate electrode to ensure that the electrons leave via the exit-gate electrode.

The energy distribution of the beam is measured using a cylindrical retarding potential analyzer (RPA). Electrons that pass through the RPA are collected on an aluminum plate, which is biased slightly positively (~ 2 V) to ensure that all of the positrons are collected. A potential bias much larger than this was avoided, since it can cause secondary electron emission from the plate, which leads to an apparent increase in the beam current. A $3 \text{ k}\Omega$ shunt resistor is used in conjunction with a voltage amplifier to measure the beam current, which is recorded on a digital oscilloscope. Care must be taken while measuring the energy distribution of the electron beam in a magnetic environment. In particular, when the beam is partially reflected by the analyzer electrode, the reflected particles interact with the incident beam, causing a space charge to build up. This increased space charge can push electrons through the RPA, which would appear as an increase in the energy spread of the beam. To minimize this effect, the retarding energy analyzer is raised for only a short time ($\sim 10 \mu\text{s}$) and then lowered to release any charge buildup. Figure 8 shows the energy distribution of a typical beam (0.10 eV FWHM) used in this experiment. Using the technique described in this section, it is possible to generate a magnetized electron beam with an energy resolution as low as 0.018 eV .^{35,36} For the experiment described here however,

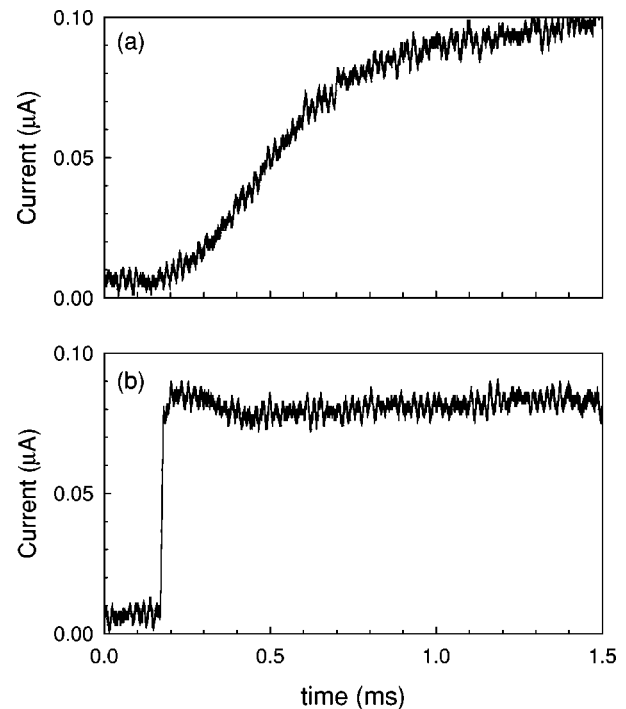


FIG. 9. Beam current extracted from a room-temperature electron plasma using (a) a linear voltage ramp to dump the plasma and (b) an optimized dump voltage waveform. Note the faster current rise ($t_r \approx 3 \mu\text{s}$) and stable current thereafter in (b).

the beam currents achievable with such a small energy spread are not sufficient to excite a measurable instability in the positron plasma. We therefore chose to use an electron beam current ($\sim 0.1 \mu\text{A}$), which is large enough to excite a measurable instability, but still small enough to measure the growth rate in the energy regime of interest.

To accurately study the electron-beam positron-plasma transit-time instability, the rise time of the electron beam current, t_r , must satisfy the condition $t_r \ll 1/\gamma$, where γ is a typical growth rate of the instability ($\sim 5 \times 10^4 \text{ s}^{-1}$), and the beam current must remain constant over the duration of the interaction. Figure 9 shows the beam current as a function of time using two different voltage ramps on the dump electrode. A simple linear ramp results in a rather slow current rise time of over 1 ms [e.g., see Fig. 9(a)], and so it is not suitable for studying the instability. A faster rise time is generated by modifying the dump waveform in the following manner. The total charge dumped from the well at any given time during the beam extraction depends only on the dump voltage at that time. Therefore, the time-integrated current (i.e., the total charge) resulting from a linear ramp beam dump can be used as an inverse lookup table to find the dump voltage required to achieve an arbitrary current waveform. Figure 9(b) shows a typical beam current waveform used in the experiment.³⁶ It is generated using the dumping procedure described above to produce a quick current rise ($t_r \approx 3 \mu\text{s}$) and $\approx 0.08 \mu\text{A}$ current thereafter.

It is also important that the beam diameter be small compared to the plasma diameter. This is accomplished by forcing the electron beam source diameter to be small compared to the positron plasma, since the extracted electron beam

diameter is directly related to the size of the electron source. To do this a 2.9 mm aperture is located in front of the hot-cathode electron gun. Figure 5 compares the radial profiles of the electron beam and positron plasma. The figure indicates an electron beam diameter $R_b \approx 2$ mm. Thus, there is little radial expansion during the beam formation process, and the electron beam's diameter is smaller than that of the plasma's, thereby fulfilling the assumptions of the model presented in Sec. II.

C. Beam–plasma experiment

The beam–plasma transit-time instability is studied in the following manner. First, a plasma of 1.6×10^7 positrons is accumulated in the cylindrical trap and transferred into the quadrupole trap. As the positron plasma cools to room temperature, the hot-cathode electron gun, which is located off axis for the positron filling phase [see Fig. 4(a)], is moved into position, and an electron plasma is accumulated in the cylindrical well. Figure 4(c) shows schematically the potential profiles generated by the cylindrical and quadrupole traps that are used to confine the electron and positron plasmas, respectively, along with the space charge of both plasmas (indicated by shading). After the electron and positron plasmas have cooled to room temperature, an electron beam is generated and magnetically guided through the positron plasma. As the electron beam traverses the positron plasma, the transit-time instability causes the center of mass oscillations to grow in amplitude. The oscillations are detected using a pickup electrode, shown in Fig. 4(b), which measures the oscillating image charge generated by the positron plasma.

After each cycle, the beam energy is adjusted by varying the potential on the exit-gate electrode of the cylindrical trap. The energy of the electron beam relative to the positron plasma is denoted in Fig. 4(c) by E_0 . The relative beam energy is the sum of eV_s and eV_t , where V_s is the space charge of the positron plasma, and V_t [which is negative in Fig. 4(c)] is the potential difference between the dump electrode of the quadrupole trap and the exit-gate electrode of the cylindrical trap. For example, if the dump and exit-gate electrodes of the quadrupole and cylindrical traps were both at the same potential, the electron beam energy through the positron plasma would be eV_s .

As we discuss in the next section, in an earlier study of the transit-time instability¹⁷ the measured growth rates were an order of magnitude larger than they are for the current experiment. Consequently, when the electron beam passed through the plasma, any noise in the plasma could act as a “seed” for the growth of the instability. In the current experiment, the lowest growth rates are not large enough to ensure that the center of mass mode can grow above the detection amplifier noise before the reservoir of electrons is depleted. In these cases, we found it essential to actively “seed” the center-of-mass mode to some small amplitude before the electron beam is turned on. This is accomplished by applying a sinusoidal signal, at the same frequency as the center of mass mode (~ 4.2 MHz), to the entrance gate of the quadrupole trap. Because of the high- Q properties of the

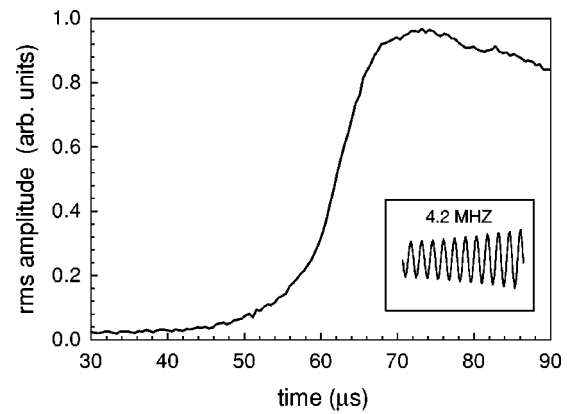


FIG. 10. A typical rms amplitude from the pickup electrode signal, showing the growth of the transit-time instability excited by an electron beam traversing a positron plasma stored in a quadrupole Penning trap. The inset shows the pickup electrode signal on an expanded time scale at 60 μ s, illustrating the individual center-of-mass oscillations at a frequency of 4.2 MHz.

quadrupole trap, the timing of the seeding is not critical, and can be done as much as a few milliseconds before the electron beam is turned on. To ensure that the seeding processes does not affect the measured growth rate, a systematic check was performed by measuring the instability growth rate with and without actively seeding the plasma in an energy regime where the seeding was not necessary.

IV. RESULTS

Figure 10 shows a typical rms signal from the pickup electrode as the electron beam passes through the positron plasma. The inset shows a 2.6 μ s long time record of the pickup electrode signal, illustrating the individual oscillations at 4.2 MHz. As discussed in Sec. II, the plasma center-of-mass mode has an oscillation frequency corresponding to that of a single positron oscillating in the potential well and is predicted to be $\omega_z/2\pi = 4.1$ MHz. The difference between the calculated and measured frequencies is likely due to small departures from the ideal quadrupole geometry.

The electron beam is turned on at $t=0$ exciting the instability in the plasma. Some time later the amplitude of the center of mass oscillations begins to grow out of the noise in the center of mass mode. After the initial exponential growth, the growth rate of the center-of-mass mode decreases, causing the amplitude of oscillation to overshoot its final value and then eventually stabilize (not shown in Fig. 10). In the earlier study of the transit-time instability,¹⁷ the initial growth phase was also followed by a decay phase. Using a γ -ray detector, it was determined that the decay in this case was due to the ejection of positrons from the quadrupole trap when the plasma oscillations became so large that they were no longer confined by the potential well. We note that the potential well confining the positrons was ~ 6 eV deep, and the electron beam energy used was only 1–2 eV, so that some of the positrons must have been accelerated to energies much larger than that of the relative beam energy. A particle-in-cell simulation confirmed this, showing that the center-of-

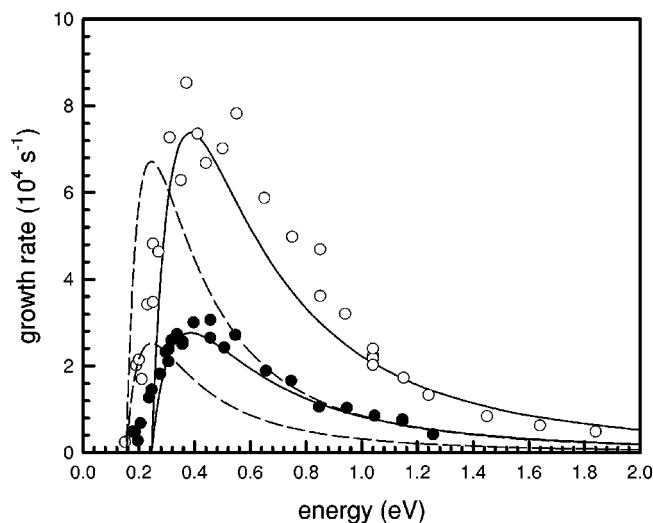


FIG. 11. Growth rates for the beam-plasma interaction in the quadrupole trap. The solid and open circles are the data using a 0.03 and 0.08 μA electron beam, respectively. The dashed and solid lines are the results of the cold-fluid theory of Sec. II with a 3.2 cm plasma diameter and a plasma aspect ratio of $\alpha=1.1$ and $\alpha=1.4$, respectively.

mass mode, could cause the ejection of positrons from the trap.¹⁷

In the present experiment, we decided to study the system in a lower growth regime, where wave saturation occurs before the particles were ejected from the trap. To accomplish this, beam currents were used that are an order of magnitude smaller than in the earlier experiment. This resulted in small-amplitude plasma oscillations. We verified using a γ -ray detector that these oscillations do not eject positrons from the potential well, and therefore the overshoot and saturation of the center-of-mass mode must be caused by an effect other than positron ejection. The most likely possibility is that nonlinear plasma effects are responsible for the observed saturation. We have not yet carried out a detailed study of the saturation, but believe that it is likely to be an interesting area of further research.

Figure 11 shows the measured instability growth rate as a function of beam energy for two beam currents. The predictions of the cold-fluid theory (i.e., Sec. II), are also shown for a fixed plasma diameter of 3.2 cm and a plasma length of 3.4 and 4.5 cm, i.e., $\alpha=1.1$ and 1.4, respectively. For a direct comparison of the results of the theory shown in Figs. 2 and 3 with the data shown in Fig. 11, we note that the range of energies studied here (i.e., 0.2–2.0 eV) corresponds to the range of scaled transit times, T , of 1.75–0.5 for $\alpha=1.1$, and 2.23–0.75 for $\alpha=1.4$. There is qualitative agreement between the theoretical and experimental results for $\alpha=1.1$, which is the aspect ratio determined by the Poisson-Boltzmann simulation and similar to the aspect ratio determined by the theory (see Sec. III A). A much better fit is obtained by adjusting the plasma length. The solid line in Fig. 11 shows the best fit, which occurs for a plasma length of 4.5 cm. Note that adjustment of only this one parameter results in good quantitative agreement between experiment and theory for both the shape and the amplitude of the growth rate at both values of electron beam current studied.

We do not have a complete understanding of the remaining discrepancies between theory and experiment. Adjusting the plasma length might be justified for two reasons. First, because the plasma length affects the beam transit time, the instability is quite sensitive to this parameter. Second, there are a number of systematic errors that make the determination of the plasma length difficult. The Poisson-Boltzmann code requires a number of input parameters to calculate the plasma density, and therefore the plasma length. These include the total positron number, positron radial profile, plasma temperature, and accurate modeling of the electrode structure. A systematic error in any of these parameters can alter the calculated length. For example, if the number of trapped positrons was larger than that measured, the plasma space charge potential would increase, thereby increasing the plasma length. However, this cannot entirely explain the results because an increase in the positron number would decrease the magnitude of the predicted growth rate, and the agreement between the theory and experiment in this respect is quite good.

Another difficulty in determining the plasma length is illustrated in Fig. 6(b). In the theory a flat-topped density profile is assumed (i.e., a cold plasma). However, this clearly does not correspond to the density profile of the experimental plasma, which is at room temperature. Thus, there is no intrinsic reason to believe that the choice of plasma length equal to the FWHM of the experimental plasma is strictly correct. Here again, this cannot entirely explain the results, because the best fit corresponds to a plasma length of 4.5 cm, which appears to be too large to fit the experimental results for the growth rate.

It is also interesting to note that by adjusting the absolute value of the beam energy, the agreement between the experimental and theoretical predictions for the $\alpha=1.1$ case is greatly improved. For example, by decreasing the assumed beam energy by 0.1 eV, a much better fit is obtained. Determining the absolute value of the beam energy relies on an accurate knowledge of the positron space charge potential and the potential difference between the exit-gate electrode and quadrupole well potential (see Fig. 4). Uncertainties in the space charge potential could cause discrepancies on the order of 0.1 eV. This implies that the discrepancy between the theory and experiment could be due to an energy offset and not to an error in the measured plasma length. We find, however, that the agreement obtained by adjusting the plasma length is still better than that obtained by adjusting the absolute energy.

To summarize, the absolute agreement between the experimental and theoretical results is reasonable, even with no fitted parameters. When the length parameter is adjusted, the agreement over the entire range of beam energies studied is quite good. The agreement with the cold-fluid theory implies that the system acts like a transit time oscillator, exciting a high- Q oscillation of the center-of-mass motion of the plasma. The theory also predicts that the instability growth rates scale linearly with beam currents, which is confirmed by the datasets taken with beam currents of 0.03 and 0.08 μA . Our previous experiments were limited by large beam energy spreads to studying the instability at beam energies

above the maximum in the growth rate. The new cold electron beam has allowed us to study the instability over the entire range of interest, from onset through the maximum growth rate and beyond.

V. POTENTIAL AREAS FOR FUTURE WORK

There are a number of experiments that can now be performed to increase our understanding of the electron-beam positron-plasma system. For example, by stabilizing the center-of-mass mode with an active feedback system,³⁷ it should be possible to measure the growth rate of higher-order modes. There may also be interesting effects at energies below the instability onset. In this energy range, cold-fluid theory predicts that there is a band of energies at which the growth rate is negative, and this should therefore have a damping effect on the center-of-mass oscillations. By exciting the center-of-mass mode to large amplitudes before the electron beam traverses the plasma, we could, in principal, study these negative growth rates.

Although this paper did not focus on the two-stream instability generated in the cylindrical trap,¹⁷ reexamining this phenomenon using the cold electron beam will likely yield interesting new insights. It is clear from the earlier experiments that the onset of the instability occurs at an energy below that which was investigated in those experiments. It should be possible to use the new cold beam to measure the heating rate for a range of positron energies from the onset of the instability through the maximum in the heating rate. Another interesting aspect of the two-stream instability is the method by which the plasma is heated. The heating is assumed to arise from the growth of unstable plasma modes that then transfer energy to the plasma particles. Direct measurements of these unstable modes should prove insightful. To measure them, a pickup electrode must be located near the plasma in order to detect the image charge generated by the (presumably short wavelength) plasma oscillations. We believe that these experiments can offer further insight into the underlying physics of the beam-plasma instability.

Unfortunately, the prospects for studying *relativistic* electron-positron plasmas, which is of keen interest to the astrophysics community, continue to be poor, at least in the intermediate term. Obtaining Debye lengths that are smaller than the plasma size, which is essential for the charge cloud to behave as a plasma, would require about five orders of magnitude more positrons than can now be accumulated. However, progress in the accumulation of positron plasmas continues. For example, the number of positrons now available is three orders of magnitude more than the first positron plasma created in 1989, and a further two orders of magnitude increase can be expected within the next few years.³⁸

VI. SUMMARY

We have investigated a beam-plasma system in a new and interesting range of beam energies, studying a transit-time instability in a positron plasma stored in a quadrupole Penning trap. Using a new technique that we developed to generate cold electron beams, we have been able to measure the growth rate of the center-of-mass mode from the onset of

the instability through the maximum in the growth rate. We also developed a detailed theoretical model of the transit-time instability. An absolute comparison of the data with the results of the cold-fluid theory shows reasonable agreement over the entire range of energies and beam currents studied.

The experiments presented here represent further studies of the electron-positron beam-plasma system. To our knowledge, these experiments are the only ones currently being conducted on this type of plasma, or on any type of equal-mass plasma. Although the techniques described here are not suitable for studying the properties of equal-mass plasmas where the species have no net currents relative to each other, this is likely to be the only experimentally accessible system available for study in the near term. Experiments of this type are likely to be of value in extending our understanding of the behavior of equal-mass plasmas. The combination of the ability to efficiently accumulate and store large numbers of positrons with the technique described here to produce cold electron beams should provide opportunities to investigate other interesting phenomena in electron-positron plasmas.

ACKNOWLEDGMENTS

We are indebted to R. W. Gould for many helpful suggestions. We thank E. A. Jerzewski for his expert technical assistance. This work is supported by the Office of Naval Research, Grant No. N000-14-97-1-0366. The contributions of D.H.E.D. were supported by the Office of Naval Research Grant No. N000-14-96-1-0239 and National Science Foundation Grant No. PHY-9876999.

¹F. C. Michel, *Rev. Mod. Phys.* **54**, 1 (1982).

²V. Tsyтович and C. B. Wharton, *Comments Plasma Phys. Controlled Fusion* **4**, 91 (1978).

³G. P. Zank and R. G. Greaves, *Phys. Rev. E* **51**, 6079 (1995).

⁴N. Iwamoto, *Phys. Rev. E* **47**, 604 (1993).

⁵G. A. Stewart, *J. Plasma Phys.* **50**, 521 (1993).

⁶J. Zhao, K. I. Nishikawa, J. I. Sakai, and T. Neubert, *Phys. Plasmas* **1**, 103 (1994).

⁷J. Sakai, M. Eda, and W. Shiratori, *Phys. Scr.* **T75**, 67 (1998).

⁸D. Gyobu, J. Sakai, M. Eda, T. Neubert, and M. Nambu, *J. Phys. Soc. Jpn.* **68**, 471 (1999).

⁹A. Dubinov, V. Selemir, and A. Sudovtsov, *Phys. Lett. A* **223**, 186 (1996).

¹⁰J. Zhao, J. I. Sakai, and K. I. Nishikawa, *Phys. Plasmas* **3**, 844 (1996).

¹¹A. D. Rogava, S. M. Mahajan, and V. I. Berezhiani, *Phys. Plasmas* **3**, 3545 (1996).

¹²L. Stenflo, P. K. Shukla, and M. Y. Yu, *Astrophys. Space Sci.* **117**, 303 (1985).

¹³T. Kitanishi, J. Sakai, K. Nishikawa, and J. Zhao, *Phys. Rev. E* **53**, 6376 (1996).

¹⁴G. Machabeli, S. Vladimirov, and D. Melrose, *Phys. Rev. E* **59**, 4552 (1999).

¹⁵V. Skarva, V. Berezhiani, and G. Carlini, *Phys. Scr.* **57**, 456 (1998).

¹⁶C. M. Surko, M. Leventhal, and A. Passner, *Phys. Rev. Lett.* **62**, 901 (1989).

¹⁷R. G. Greaves and C. M. Surko, *Phys. Rev. Lett.* **75**, 3846 (1995).

¹⁸T. M. O'Neil, *Comments Plasma Phys. Controlled Fusion* **5**, 213 (1980).

¹⁹T. Intrator, N. Hershkovitz, and R. Stern, *Phys. Fluids* **26**, 1942 (1983).

²⁰J. P. Schermann and F. G. Major, *Appl. Phys.* **16**, 225 (1978).

²¹S. J. Gilbert, R. G. Greaves, and C. M. Surko, *Phys. Rev. Lett.* **82**, 5032 (1999).

²²J. Walz, C. Zimmermann, L. Ricci, M. Prevedelli, and T. W. Hansch, *Phys. Rev. Lett.* **75**, 3257 (1995).

²³H. Boehmer, M. Adams, and N. Rynn, *Phys. Plasmas* **2**, 4369 (1995).

- ²⁴R. G. Greaves and C. M. Surko, Phys. Plasmas **4**, 1528 (1997).
- ²⁵T. Stringer, Plasma Phys. **6**, 267 (1964).
- ²⁶O. Heil and A. Arsenjewa-Heil, Z. Phys. **95**, 752 (1935).
- ²⁷J. Muller, Hochfrequenztechnik und Elektroakustik **41**, 156 (1933).
- ²⁸J. P. Freidberg and D. W. Hewett, J. Plasma Phys. **26**, 177 (1981).
- ²⁹C. Kuyatt and J. Sympton, Rev. Sci. Instrum. **38**, 103 (1967).
- ³⁰C. S. Weimer, J. J. Bollinger, F. L. Moore, and D. J. Wineland, Phys. Rev. A **49**, 3842 (1994).
- ³¹D. H. E. Dubin and T. M. O'Neil, Rev. Mod. Phys. **71**, 87 (1999).
- ³²T. J. Murphy and C. M. Surko, Phys. Rev. A **46**, 5696 (1992).
- ³³A. P. Mills, Jr. and E. M. Gullikson, Appl. Phys. Lett. **49**, 1121 (1986).
- ³⁴R. G. Greaves, M. D. Tinkle, and C. M. Surko, Phys. Plasmas **1**, 1439 (1994).
- ³⁵S. J. Gilbert, C. Kurz, R. G. Greaves, and C. M. Surko, Appl. Phys. Lett. **70**, 1944 (1997).
- ³⁶C. Kurz, S. J. Gilbert, R. G. Greaves, and C. M. Surko, Nucl. Instrum. Methods Phys. Res. B **143**, 188 (1998).
- ³⁷P. Tham, A. Sen, A. Sekiguchi, R. G. Greaves, and G. A. Navratil, Phys. Rev. Lett. **67**, 404 (1991).
- ³⁸C. M. Surko, S. J. Gilbert, and R. G. Greaves, in *Non-Neutral Plasma Physics III*, edited by J. J. Bollinger, R. L. Spencer, and R. C. Davidson (American Institute of Physics, Melville, NY, 1999), pp. 3–12.